



**HAL**  
open science

# Analysis of the Li-ion Batteries Modeling Choices For Microgrid Design

Corentin Boennec, Lucas de Oliveira Albuquerque, Bruno Sareni, Fabien  
Lacressonnière, Sandra Ulrich Ngueveu

► **To cite this version:**

Corentin Boennec, Lucas de Oliveira Albuquerque, Bruno Sareni, Fabien Lacressonnière, Sandra Ulrich Ngueveu. Analysis of the Li-ion Batteries Modeling Choices For Microgrid Design. International Conference on Electrical Sciences and Technologies in Maghreb (CISTEM), Oct 2022, Tunis, Tunisia. hal-03895725

**HAL Id: hal-03895725**

**<https://ut3-toulouseinp.hal.science/hal-03895725>**

Submitted on 13 Dec 2022

**HAL** is a multi-disciplinary open access archive for the deposit and dissemination of scientific research documents, whether they are published or not. The documents may come from teaching and research institutions in France or abroad, or from public or private research centers.

L'archive ouverte pluridisciplinaire **HAL**, est destinée au dépôt et à la diffusion de documents scientifiques de niveau recherche, publiés ou non, émanant des établissements d'enseignement et de recherche français ou étrangers, des laboratoires publics ou privés.

# Analysis of the Li-ion Batteries Modeling Choices For Microgrid Design

Corentin Boennec, Lucas de Oliveira Albuquerque, Bruno Sareni, Fabien Lacressonnière, Sandra Ulrich Ngueveu\*

LAPLACE, UMR CNRS-INPT-UPS, Université de Toulouse, France

\*LAAS-CNRS, Université de Toulouse, CNRS, INP, Toulouse, France

{boennec, albuquerque, sareni, fablac}@laplace.univ-tlse.fr, ngueveu@laas.fr

**Abstract**—This paper presents different Li-ion battery models integrating energy efficiency and aging in the frame of microgrid design. More specifically, it compares the quantitative and qualitative differences of the models considering multiple sizings and scenarios associated with a simple microgrid. It also investigates the impacts of each model on two techno-economic criteria: the renewable energy share and net present value related to the microgrid.

**Index Terms**—Index Terms : Battery Storage, Aging, Microgrids, Modeling

## I. INTRODUCTION

The integration of renewable energy into electricity generation systems has recently become essential to reduce the carbon impact in view of the current climate challenges, especially in the context of smart microgrids. The design of these networks has generally been addressed via optimization problems that aim to minimize the sum of two costs, the investment cost and the operating cost (CAPEX and OPEX) while ensuring a certain level of self-sufficiency [1]. It turns out that performing this optimization requires modeling the system and by extension all its elements/components. In this paper, the influence of the accuracy level of Li-ion battery models are studied in order to identify the best compromise between complexity and accuracy. Several models from the literature [2]–[7] will be explored and analyzed, integrating in a coupled or decoupled way energy efficiency and aging.

## II. MODELS DESCRIPTION

### A. The temporal model

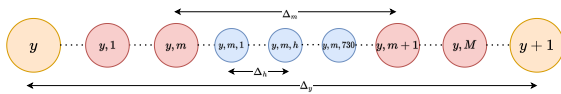


Fig. 1. Temporal model and link between scales.

Our temporal model includes three time scales addressing different missions. A fine scale modeled by an hourly step to capture the intra-day dynamics of the system, as well as a long scale with an annual step for investment management and finally a monthly time scale to update our cycle based aging

Authors declare no competing interests

models. The link that is made between these time scales can be seen in Fig. 1.

The set of hours, months and years are then respectively defined as  $h \in \mathbb{H} = \{1..H\}$ ,  $m \in \mathbb{M} = \{1..M\}$ ,  $y \in \mathbb{Y} = \{1..Y = 20\}$ , with a  $\Delta_h, \Delta_m$  and  $\Delta_y$  time-step verifying  $\Delta_y = 12 \cdot \Delta_m = 8760 \cdot \Delta_h$ .

### B. The energy model

The energy model controls the state of charge (SoC  $\in [0, 1]$ ) of the battery during its interaction with the system. Specifically, here the batteries are operated within the limit of  $SoC^{min} = 0.2$  and  $SoC^{max} = 0.8$ .

To conduct our study, a linear model with constant efficiency has been implemented. This model from [2] has few parameters: the efficiency  $\eta$  and the nominal capacity  $E^{nom}$  of the battery in [kWh].

$$SoC_{h+1} = SoC_h - \frac{(\eta \cdot P_h^{ch} - \eta^{-1} \cdot P_h^{dch}) \cdot \Delta_h}{E^{nom}} \quad (1)$$

Equation (1) governs the battery SoC at hourly intervals  $\Delta_h$ , where  $P_h^{ch} \leq 0$  and  $P_h^{dch} \geq 0$  respectively denotes the Li-ion charge/discharge power at hour  $h$ . Those variables do not coexist, meaning if one is non-zero the other one is.

### C. The aging models

The aging models control the state of health of the battery ( $SoH \in [0, 1]$ ) during its interactions with the system. They define the appropriate time to replace the degraded battery. In this study the replacement threshold corresponding to the battery End Of Life (EOL) is set to 80%, which means the battery is replaced when SoH falls below 80% (we know that stationary storage can be pushed to around 40%). However, the models used in this study do not take account of the rapid degradation phase. Furthermore, since the rate of degradation increases substantially shortly after our 80% threshold, with the curve forming a "knee" [8], we believe it is best to limit this study to an area for which aging is better known.

For this study, 4 aging models have been implemented. They are presented in an increasing order of captured aging dynamics.

1) *Fixed lifetime model (FL)*: This first model simply assumes that the battery has a fixed lifetime. At the end of its life, the SoH drops from 100% to EOL, and the battery is replaced.

The next three models implement at least a cycle aging related to battery usage and a calendar aging associated with the elapsing time. While the cycling degradation model is different for each aging model, the calendar degradation model is common to all of them and expressed as a linear degradation extracted from the time stress function of [5] and similar to [6].

$$\Delta_{cal}(t) = 1 - e^{t \cdot c_{cal}} \quad (2)$$

with  $c_{cal} = 1.49 \cdot 10^{-6}$  and  $t$  being the time in hours.

2) *Exchanged Energy model (EE)*: In this second model from [3] the battery state of health is a function of a total amount of exchangeable energy and the part of it already exchanged. The maximum exchangeable energy  $E_{tot}^{ex}$  depends on the achievable number of cycles  $N_{tot}^{cycle}$  for a fixed Depth of Discharge (DoD) and on the total capacity of the battery  $E^{nom}$ ,

$$E_{tot}^{ex} = 2 \cdot N_{tot}^{cycle} \cdot DoD^{max} \cdot E^{nom} \quad (3)$$

where  $DoD^{max}$  is the maximum depth that a half cycle (charge or discharge) can reach. It is calculated via:

$$DoD^{max} = SoC^{max} - SoC^{min} \quad (4)$$

In order to determine the parameter  $N_{tot}^{cycle}$  we use the *number of cycle-to-failure* (NCF) curve from [5] giving the number of cycle before reaching  $EOL = 80\%$ . Thus, thanks to this curve, we obtain  $N_{EOL}^{cycle}$  verifying the following relation  $N_{tot}^{cycle} \times (1 - EOL) = N_{EOL}^{cycle}$ . The hourly cycle degradation is then computed according to the following equation with  $P_h$  being Li-ion charge/discharge power in hour  $h$ .

$$\Delta_{cyc}(h) = \frac{P_h \cdot \Delta_h}{E_{tot}^{ex}} \quad (5)$$

The SoH is finally computed as:

$$SoH_{h+1} = SoH_h - \Delta_{cyc}(h) - \Delta_{cal}(\Delta_h) \quad (6)$$

3) *Rainflow model (RF)*: In this model inspired by [4] the per cycle degradation is evaluated by a Rainflow count. The method consists in calculating a fatigue as a function of a SoC profile  $\overrightarrow{SoC}$ , in order to update the SoH. More precisely, the total fatigue is obtained by adding the fatigue associated to each half-cycle (charge or discharge) of the profile. The induced fatigue is a function of the depth of the half-cycle in question. In order to collect this profile, the calculation of this fatigue is periodically performed once a month (every  $\Delta_m$ ). The  $\overrightarrow{SoC}_{y,m}$  profile of the previous month SoC must be processed to extract a vector containing the DoD of each half-cycle performed during that month. Further explanation of this process can be found in [4].

The value of the fatigue generated during the past month is then obtained via (7) where  $\overrightarrow{DoD}$  is the vector of DoDs associated with the SoC profile:

$$\Delta_{cyc}(m) = \sum_{i=1}^{|\overrightarrow{DoD}|} \frac{1}{2 \cdot NCF(\overrightarrow{DoD}_i)} \quad (7)$$

The factor 2 in the denominator comes from our choice to consider half-cycles, while the  $NCF$  function provides, via the  $NCF$  curve associated with the battery and generally supplied by the manufacturer, the number of cycles achievable for a given DoD before EOL.

Finally, adding the calendar degradation gives us this final equation for monthly update:

$$SoH_{m+1,h} = SoH_{m,H} - \Delta_{cyc}(m) - \Delta_{cal}(\Delta_m) \quad (8)$$

4) *Semi-Empirical Model (SE)*: This model from [5] incorporates empirical and physical degradation parameters. It differs from other models because it takes account of the electro-chemical reaction taking place within the battery at the beginning of its life, caused by the consumption of Lithium ions and electrolyte solvents which form the passivation layer called Solid Electrolyte Interphase (SEI). This layer is essential for the longevity of the battery, as it protects the graphite from direct contact with the electrolyte, but continues to grow and thus degrades the battery capacity during its life [9].

The general formula to compute the degradation for a new battery is given by :

$$SoH_t = \alpha_{sei} \cdot e^{-\beta_{sei} \cdot fd_t} + (1 - \alpha_{sei})e^{-fd_t} \quad (9)$$

with  $fd_t$  being the global stress undergone by the battery until time  $t$  and depending on 4 parameters: the average depth of discharge  $\overrightarrow{DoD}$ , the elapsed time  $t$ , the average state of charge  $\overrightarrow{SoC}$  and the temperature  $T$ . Hence we consider  $fd^{unit}$  as the unit equivalent associated with a single half-cycle. Therefore we define  $fd_t$  as the sum of  $fd^{unit}$  for each half-cycle up to the instant  $t$ .  $fd^{unit}$  is calculated via the following equation:

$$fd^{unit} = [0.5 \cdot S_{DoD}(DoD) + S_t(t)] \cdot S_{SoC}(\overrightarrow{SoC}) \cdot S_T(T) \quad (10)$$

where  $S_x$  are the stress functions defined in [5] which allows the calculation of the stress associated with each parameter.

In this work, the influence of the temperature is not taken into account. Hence, the temperature stress function is equal to 1 ( $T = T_{ref}$ ) during the simulation. We are aware of its primordial nature (as stated e.g in [10]) and choose to assume that in a stationary environment temperature can and should be kept as close as possible to  $T_{ref} = 298.15K$ .

5) *Calibration of models for meaningful comparison*: In order to make our models comparable, we have chosen to configure them using common data. The main resource is the  $NCF$  curve for a NMC battery of [5] used to parameterize the cycling degradation of *Rainflow* and *Semi-Empirical* models. Finally, for the *Exchanged Energy* model, we take from this  $NCF$  curve the number of cycles achievable for a DoD of 60% ( $DoD^{max}$ ), thus obtaining the parameter  $N_{EOL}^{cycle}$ .

#### D. Coupling between energy models and aging models

4 types of coupling are considering as follow :

- The absence of coupling.
- The energy (E) coupling, which induces a loss of capacity for the battery and defined as follows:  $E(t) = E^{ini} \cdot SoH_t$ .
- The internal resistance (R) coupling, which induces a loss of efficiency by a linear decrease as proposed in [6] or [7] via:  $\eta(SoH_h) = \eta^{ini} - \frac{1-SoH_h}{4}$  with an initial efficiency  $\eta^{ini}$  of 95%.
- The E and R (ER) coupling which applies both simultaneously.

### III. DESCRIPTION OF OUR CASE STUDY

#### A. The microgrid

We consider a microgrid with storage represented in Fig. 2 to observe the impacts of the battery modeling on the various techno-economic indicators. The choice of a simple case study operated with a trivial management policy allows us to conduct our analyses over a 20-year horizon with an hourly time step. The system sizing variables are:

- $E_{bat}$  [kWh]: The battery size.
- $P_{pv}$  [kWp]: The peak power of the photovoltaic panel.
- $P_{sub}$  [kVA]: The subscribed power which, if exceeded, will generate additional costs.

#### B. Techno-economical metrics

We evaluate the system from two main indicator, the cost of the system and its self-sufficiency level.

1) *Renewable Energy Share (RES)*: The solar production share is a metric of the system self-sufficiency, it measures the share of energy supplied by the PV panel in the total energy consumption of the system. Since the system has two possible suppliers, PV panel or grid, this share is obtained from its complement (the grid share) :

$$RES = 1 - \frac{\sum P^{g,+}}{P^{load}} \quad (11)$$

2) *System costs*: The cost metric used in this study is the Net Present Value (NPV). For its calculation we define  $C_y^i$ ,  $C_y^o$ , respectively the investment and operating costs for year  $y$ .  $C_Y^s$  is the residual value of the equipment, calculated at the end of the time horizon  $y = Y$  (non-zero only for  $y = Y$ ).

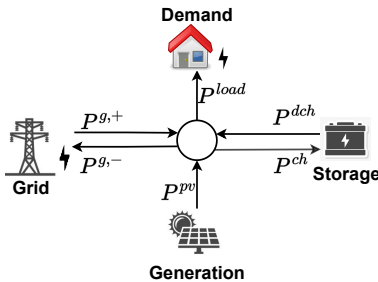


Fig. 2. Simplified diagram with power flows of our microgrid.

For the battery, a linear decrease of its value is considered, reaching 0% at EOL. Finally, the discount rate is set at 4.5%. We deliberately exclude from the calculation the cost  $C_y^{base}$  (the cost of meeting demand over the simulation horizon by relying exclusively on the grid) because it is independent of the battery modeling choices. The modified NPV, NPV\* is then defined by (12).

$$NPV^* = \sum_{y=1}^Y \frac{(-C_y^i - C_y^o + C_y^s)}{(1 + \tau)^y} \quad (12)$$

#### C. Key data associated with costs

- Subscription cost (made continuous by inter/extrapolation for analysis purposes): 6 to 36 kVA for 144 to 494 €/year
- Electricity tariffs VAT included for peak hours (with a 0.75 factor for off-peak hours) : 0.19 €/kWh.
- Cost of exceeding the subscription limit per hour of excess: 11.11 €
- Cost of PV cells: 1300 €/kWp [11]
- Cost of the Li-ion cells : 300 €/kWh [11]
- Selling price : 0.01 €/kWh

#### D. Details about our simulation environment

In order to simulate the use of the microgrid and be able to carry out analysis on our models, we use a set of 20-year scenarios with an hourly time step. They provide for each hour the energy demand and solar radiation. Their generation is done according to the method described in [12] with data from *Ausgrid* of 20 consumers over the years 2010 to 2012.

Battery energy operation is performed as follows:

- In case of surplus ( $P_h^{load} - P_h^{pv} < 0$ ) the battery is charged. If its SoC is above  $SoC^{max}$ , the difference is sold to the grid.
- In case of a deficit ( $P_h^{load} - P_h^{pv} > 0$ ) the battery is discharged. The grid takes over if it reaches  $SoC^{min}$ .

Finally, we need to provide its sizing parameters. Assuming that the magnitude of the observed effects may depend on the size of the assets, the subscribed power  $P_{sub}$  is fixed at 10 kVA and the values of the couple  $(P_{pv}, E_{bat})$  are generated by a Sobol sequence whose bounds are  $min = (5,10)$ ,  $max = (50,80)$  in order to cover the space under consideration as uniformly as possible despite a small number of sizings. Thus 64 designs are generated. By associating these sizings to our scenarios, we provide a set of 512 input configurations (64 sizings x 8 scenarios) to simulate the microgrid.

## IV. RESULTS

#### A. Comparison of Aging models on Artificial SoC profiles

In this section, aging models are compared according to the artificial SoC profiles of Fig 3. Those profiles which are voluntary simple allows characterizing the effect of the following variables related to the cycles: average state of charge, depth of discharge and frequency.

Fig. 4 shows the strong effect of the average SoC only modeled in the *Semi-Empirical* model in which, above the reference value (here set to 0.5) accelerates aging, while on the

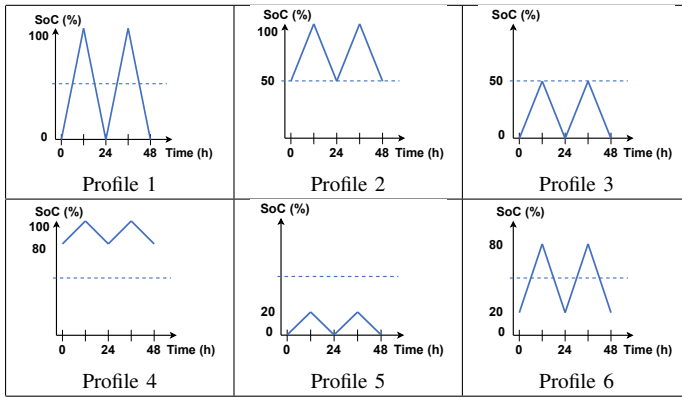


Fig. 3. Artificial SoC profiles over 48 hours - Profiles 7-12 have the same amplitude as 1-6 but twice the frequency.

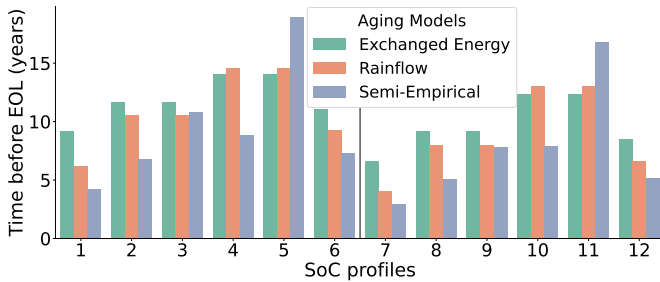


Fig. 4. Lifetime before reaching EOL of batteries undergoing artificial SoC profiles from Fig. 3.

contrary, is slowed down when the battery is operated below the reference value. Best example are comparing profiles 2 with 3 and 4 with 5.

Note that if, out of all the profiles, the *Semi-Empirical* model is generally the one with the shortest lifetime, it is because it incorporates an additional irreversible degradation due to the formation of the SEI. The only cases contradicting this statement are those where this effect is compensated by the effect of the average SoC mentioned in the previous paragraph. This is observable on profiles 3 and 5 as well as their equivalent 9 and 11.

Because *Semi-Empirical* model is taking account of all the aging factors considered in this study, its ER coupled version is hereafter taken as a reference model. Now that we have observed how the models react to artificial profiles depending on their aging factors, let us observe the impact of coupling on those factors.

### B. Impact of coupling on aging factors

In order to explain the potential impact of model coupling, a linear SoH degradation of 10% per year was staged and substituted for the aging models. This was done in order to observe the evolution of the influencing factors of our aging models and the techno-economic indicators under the effect of the different couplings. The above-mentioned influencing factors are the amount of exchanged energy, the DoD and the average SoC. Although the EOL of the battery is set to 80%, we observe these effects over the interval  $SoH \in [100\%, 40\%]$

in order to further understand the dynamics. The intervals are plotted to visualize the extent to which these effects can vary due to the simulation input parameters.

All following results in this section are expressed as a percentage change from a baseline, in this case the absence of coupling. In addition, it may be confusing, but a DoD of 30% undergoing a 10% growth due to coupling will result in a DoD of 33%.

1) *Battery Exchanged Energy*: Fig. 5 shows an almost perfect correlation between the amount of energy exchanged with the capacity of the battery due to E coupling. As expected, when capacity decreases, storage is reduced and thus the amount of energy stored and subsequently delivered also decreases. The energy exchanged by the battery is not really affected by the efficiency, the effect is even further reduced when the two couplings are combined.

2) *Cycle Depth of Discharge*: Fig. 6 shows that for a consistent annual demand, the decrease in capacity caused by E coupling leads to an increase in DoD. The increase appears relatively linear, however the impact on battery life is superlinear, with higher cycles resulting in greater fatigue per percent of DoD.

3) *Cycle Mean SoC*: Fig. 7 shows opposite effects on the average SoC, with E coupling leading to an increase and R coupling to a decrease. The variations caused by these couplings remain very small, however, the fact that they compensate each other almost nullifies the ER coupling effect.

4) *Energy Purchased*: This section studies the impact of a techno-economic influence factor. Indeed, one can expect that the decrease in capacity and therefore in the energy exchanged leads to an increase in the energy purchased and thus in the cost. This can be seen in Fig. 8 which shows an opposite effect to the one observed in Fig. 5. It is logical that for years with the same demand, a decrease in the amount of energy exchanged results in a similar increase in energy purchased. In addition, the grid has to compensate the missing energy due to the decrease in efficiency caused by R coupling.

It is noticeable that the intensity of the E coupling depends on sizing while the intensity of R coupling mostly does not (see the interval bands in Fig. 5 to 8). Also it is important to keep in mind that the intensification of an impact factor by decreasing the SoH creates a positive feedback loop, also known as a snowball effect (e.g. Rainflow, with the DoD). However, the opposite effect can also exist, e.g. the Exchanged Energy model where the feedback is negative, with aging causing the amount of exchanged energy to decrease.

### C. Measuring the deviation from a reference

Here we measure the gaps in the assessment of the techno-economic indicators of our models in comparison with a reference. The chosen reference is the *Semi-Empirical* aging model with the ER coupling for aforementioned reasons, see Section IV-A) We measure the percentage deviation from the reference, according to different metrics. For each model configuration (aging, coupling), 512 simulations are performed. It is important to remember that the cost results could be

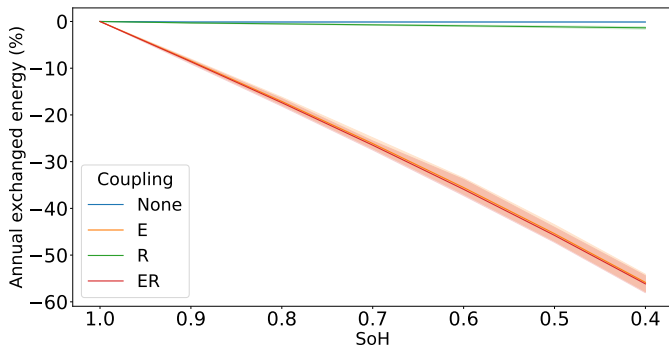


Fig. 5. Impact (%) of couplings on the amount of yearly energy exchanged by the battery.

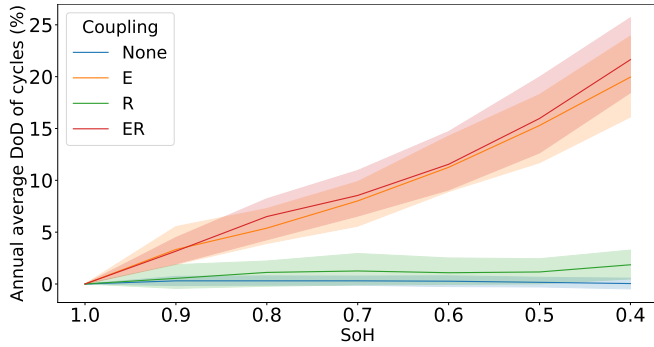


Fig. 6. Impact (%) of couplings on the yearly averaged cycle DoD.

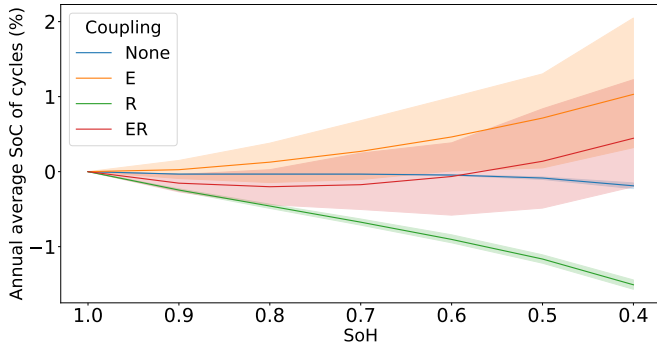


Fig. 7. Impact (%) of couplings on the the average SoC of cycles.

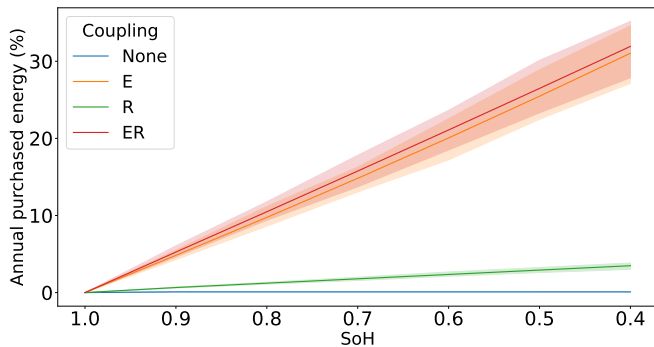


Fig. 8. Impact (%) of couplings on the amount of energy purchased.

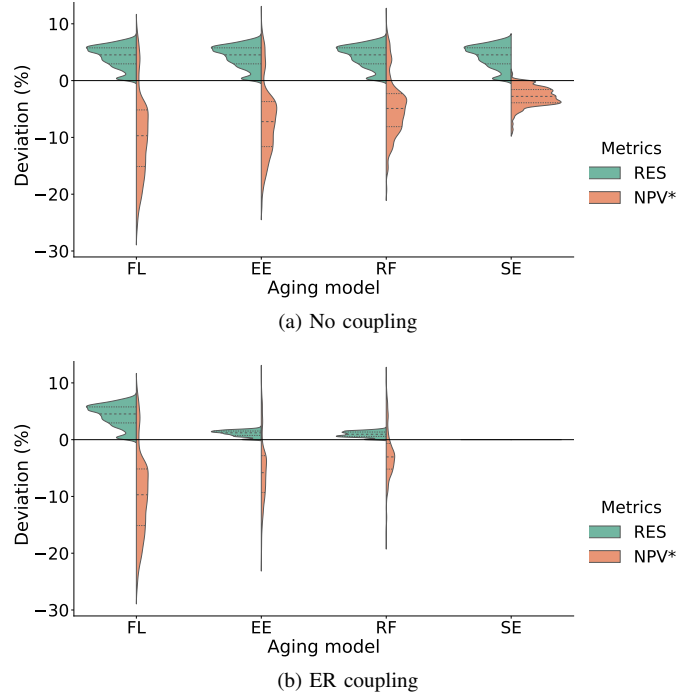


Fig. 9. Distribution of the deviation in percentage from the reference for different models and computed as :  $\frac{(val-ref) \cdot 100}{ref}$ . The horizontal dotted lines represent the quartiles.

different with other input values (for the price of battery cells, or grid prices for example). Nevertheless, we try to show the kind of effect that could be expected by modeling batteries with different levels of accuracy.

Fig. 9 displays part of our results, firstly it shows that the metric mainly impacted by the level of modeling seems to be the NPV\*. Meanwhile the RES is mainly affected by the choice of incorporating or not the coupling.

Secondly, we observe that the dispersion of the deviations for the cost metric is quite large and that its amplitude increases when the models incorporate fewer features, up to approximately  $[-25, +10]\%$  with the *Fixed Lifetime* model. The deviation can be positive or negative although it is mostly negative. Not incorporating the coupling increases the trend towards the negative part. This results in an underestimation of the cost due to an overestimation of the life expectancy of the battery, which ultimately leads to an increased amount of purchased energy (as shown in Fig. 8) as well as fewer replacements (or a higher salvage value).

Finally we can measure the effect of modeling the coupling alone by comparing the reference to its equivalent without coupling.

#### D. Quantitative differences but qualitative similarities?

The quantitative deviations of the battery models investigated in the paper have been characterized in the previous section with regard to the RES and NPV\* criteria. We now examine the qualitative differences of those models with respect to the microgrid configurations and real scenarios of Section III-D. For each model, 512 simulations are carried out

and sorted in ascending order of the considered criterion (i.e. RES or NPV\*). The similarity of the rankings between two models  $i$  and  $j$  is estimated using the Spearman correlation defined as follows:

$$r_{ij} = 1 - \frac{6}{n(n^2 - 1)} \sum_{k=1}^n d_k^2 \quad (13)$$

where  $n = 512$  is the total number of tests and  $d_k$  denotes the difference between two rankings in the sorts. A value of  $r_{ij}$  close to 1 indicates similar rankings (i.e. same behavior between models  $i$  and  $j$ ) while a value of  $r_{ij}$  close to 0 means that both models are totally uncorrelated.

TABLE I  
SPEARMAN CORRELATION COEFFICIENT FOR COST (NPV\*) RANKINGS BETWEEN CONFIGURATIONS. LEGEND:  $\emptyset$  IS THE ABSENCE OF COUPLING AND ER MEANS BOTH COUPLINGS (E AND R)

Model	FL		EE		RF		SE		
	Coupl.	$\emptyset$	ER	$\emptyset$	ER	$\emptyset$	ER	$\emptyset$	ER
FL	$\emptyset$	1							
	ER	1	1						
EE	$\emptyset$	.96	.96	1					
	ER	.97	.97	.98	1				
RF	$\emptyset$	.97	.97	.98	.99	1			
	ER	.95	.95	.99	.98	.98	1		
SE	$\emptyset$	.90	.90	.95	.94	.93	.95	1	
	ER	.88	.88	.94	.93	.92	.94	.99	1

Table I compares 8 battery aging models with respect to the  $r_{ij}$  coefficient and NPV\* criterion. It can be seen that Spearman coefficients are relatively high leading to similar behaviors. Without surprise, the lowest coefficient is between the fixed lifetime model (considered as the less quantitatively accurate) and the *Semi-Empirical* model (supposed to be the most quantitatively accurate). Nevertheless, it should be noted that this conclusion may depend on the choice of the economic factors considered. This result should be confirmed by an additional study of economic factor sensitivity but it is not within the scope of the paper. The results of the Spearman coefficient associated with the RES are not displayed because all values are higher than 0.99 which implies a perfect similarity between all models. This can be justified by the small quantitative differences and low dispersion noted for that criterion in Fig. 9.

## V. CONCLUSION

In this paper, several battery models integrating energy efficiency and aging have been compared in the frame of microgrid design. In particular, the quantitative and qualitative differences have been analyzed for a simple microgrid with respect to the RES and NPV\* criteria considering artificial and real SoC profiles. Results show that the *Semi-Empirical* model is probably the most accurate reference including various aging effect (SEI degradation, mean of SOC cycles, cycle frequency). However, the similar trend and behavior noted from the qualitative study suggest that it can be substituted by the exchangeable energy model avoiding the cycle counting which can drastically increase the CPU time and the nonlinear

features in a microgrid optimization process. We will try to verify this hypothesis in the perspective of this paper by investigating the optimal design of a simple microgrid with each model. The present study will also be extended to more refined energy models such as the tremblay-Dessaint battery model [13] including aging, loss of capacity and loss of efficiency.

## REFERENCES

- [1] E. Cuisinier, C. Bourasseau, A. Ruby, P. Lemaire, and B. Penz, "Techno-economic planning of local energy systems through optimization models: a survey of current methods," *International Journal of Energy Research*, vol. 45, no. 4, pp. 4888–4931, Mar. 2021. DOI:10.1002/er.6208
- [2] P. Carpentier, J.-P. Chancelier, M. De Lara, and T. Rigaut, "Algorithms for two-time scales stochastic optimization with applications to long term management of energy storage," Feb. 2019, working paper or preprint. [Online]. Available: <https://hal.archives-ouvertes.fr/hal-02013969>
- [3] H. Bindner, T. Cronin, P. Lundsager, J. F. Manwell, U. Abdulwahid, and I. Baring-Gould, "Lifetime Modelling of Lead Acid Batteries," p. 82, 2005.
- [4] Y. Shi, B. Xu, Y. Tan, D. Kirschen, and B. Zhang, "Optimal Battery Control Under Cycle Aging Mechanisms in Pay for Performance Settings," *arXiv:1709.05715 [cs, math]*, Jul. 2018.
- [5] B. Xu, A. Oudalov, A. Ulbig, G. Andersson, and D. S. Kirschen, "Modeling of Lithium-Ion Battery Degradation for Cell Life Assessment," *IEEE Transactions on Smart Grid*, vol. 9, no. 2, pp. 1131–1140, Mar. 2018. DOI:10.1109/TSG.2016.2578950
- [6] W. Vermeer, G. R. Chandra Mouli, and P. Bauer, "Optimal Sizing and Control of a PV-EV-BES Charging System Including Primary Frequency Control and Component Degradation," *IEEE Open Journal of the Industrial Electronics Society*, pp. 1–1, 2022. DOI:10.1109/OJIES.2022.3161091
- [7] E. Redondo-Iglesias, P. Venet, and S. Pelissier, "Efficiency Degradation Model of Lithium-ion Batteries for Electric Vehicles," *IEEE Transactions on Industry Applications*, p. 11, 2019.
- [8] P. M. Attia, A. Bills, F. B. Planella, P. Dechent, G. d. Reis, M. Dubarry, P. Gasper, R. Gilchrist, S. Greenbank, D. Howey, O. Liu, E. Khoo, Y. Preger, A. Soni, S. Sripad, A. G. Stefanopoulou, and V. Sulzer, "'Knees" in lithium-ion battery aging trajectories," *Journal of The Electrochemical Society*, vol. 169, no. 6, p. 060517, Jun. 2022. DOI:10.1149/1945-7111/ac6d13
- [9] M. B. Pinson and M. Z. Bazant, "Theory of SEI Formation in Rechargeable Batteries: Capacity Fade, Accelerated Aging and Lifetime Prediction," *Journal of The Electrochemical Society*, vol. 160, no. 2, pp. A243–A250, 2013. DOI:10.1149/2.044302jes
- [10] W. Vermeer and P. Bauer, "A Comprehensive Review on the Characteristics and Modeling of Lithium-Ion Battery Aging," *IEEE Transactions on Transportation Electrification*, vol. 8, no. 2, p. 28, 2022.
- [11] I. Petkov and P. Gabrielli, "Power-to-hydrogen as seasonal energy storage: an uncertainty analysis for optimal design of low-carbon multi-energy systems," *Applied Energy*, vol. 274, p. 115197, Sep. 2020. DOI:10.1016/j.apenergy.2020.115197
- [12] H. Radet, B. Sareni, and X. Roboam, "Generation of energy demand and pv production profiles based on markov chains for the design and operation of microgrids," *14th International Conference of TC-Electrimacs Committee, Nancy, France, 2022*.
- [13] O. Tremblay and L.-A. Dessaint, "Experimental Validation of a Battery Dynamic Model for EV Applications," *World Electric Vehicle Journal*, vol. 3, no. 2, pp. 289–298, Jun. 2009. DOI:10.3390/wevj3020289